Device and morphological engineering of organic solar cells for enhanced charge transport and photovoltaic performance

Nirmal Adhikari
Devendra Khatiwada
Ashish Dubey
Qiquan Qiao

Device and morphological engineering of organic solar cells for enhanced charge transport and photovoltaic performance

Nirmal Adhikari, Devendra Khatiwada, Ashish Dubey, and Qiquan Qiao*
South Dakota State University, Center for Advanced Photovoltaics, Department of Electrical
Engineering and Computer Science, Brookings, South Dakota 57007, United States

Abstract. Conjugated polymers are potential materials for photovoltaic applications due to their high absorption coefficient, mechanical flexibility, and solution-based processing for low-cost solar cells. A bulk heterojunction (BHJ) structure made of donor–acceptor composite can lead to high charge transfer and power conversion efficiency. Active layer morphology is a key factor for device performance. Film formation processes (e.g., spray-coating, spin-coating, and dip-coating), post-treatment (e.g., annealing and UV ozone treatment), and use of additives are typically used to engineer the morphology, which optimizes physical properties, such as molecular configuration, miscibility, lateral and vertical phase separation. We will review electronic donor–acceptor interactions in conjugated polymer composites, the effect of processing parameters and morphology on solar cell performance, and charge carrier transport in polymer solar cells. This review provides the basis for selection of different processing conditions for optimized nanomorphology of active layers and reduced bimolecular recombination to enhance open-circuit voltage, short-circuit current density, and fill factor of BHJ solar cells. © *2015 Society of Photo-Optical Instrumentation Engineers (SPIE)* [DOI: 10.1117/1.JPE.5.057207]

1 Introduction

Humanity has already faced consequences of wide use of nonrenewable natural resources. Global warming and ozone depletion, caused by the emissions of greenhouse gases during the burning of fossil fuels, as well as air pollution and soil erosion, are only several examples of irreversible changes in the environment. This clearly highlights the need for a pollution-free, renewable source of energy, hopefully in the near future, to minimize the adverse impacts to our Earth. Some renewable energy sources, such as wind, hydro, biomass, geothermal, and solar, are replacing conventional fossil fuel technology. However, these have certain limitations, such as low wind strength and increase in methane gas, which is harmful to the ozone layer. So the search for more environmentally friendly, sustainable, and inexpensive renewable energy has led researchers and the industry's interest toward photovoltaic solar energy.

Inorganic photovoltaics (PVs) constitute a matured technology having industrial and large market potentials. Traditional crystalline silicon solar cells dominate a major portion of the global PV market. However, the cost for this type of solar cell is very expensive and needs government subsidies. This might be one of the reasons for the small (~0.1%) portion of energy attributed to solar compared to global electricity generation.[1,2] Organic PVs have the potential to produce cheap and affordable energy with ubiquitous energy resources.

Organic PVs have attractive attributes, such as low cost, mechanical flexibility, light weight, abundancy, sustainability, environment friendliness, and manufacturing ease on large-area flexible substrates.[3–8] Bulk heterojunction (BHJ) polymer solar cells comprising an interpenetrating

*Address all correspondence to: Qiquan Qiao, E-mail: Qiquan.Qiao@sdstate.edu

network of a photoactive conjugated polymer (an electron donor) and a fullerene derivative (an electron acceptor) provide an efficient interfacial area for exciton dissociation and a bicontinuous pathway for effective charge transport. Photons are absorbed in the conjugated polymer resulting in the generation of excitons that diffuse to the interface between the polymer and fullerene derivative. The generated excitons dissociate at the interface into electrons and holes, in which electrons are accepted by the fullerene derivative.[9]

Poly(2-methoxy-5-(2-ethyl-hexyloxy)-1,4-phenylene vinylene) (MEH-PPV) was used as a BHJ solar cell for first time in 1995 (Ref. [10]) as a donor and fullerene derivative phenyl-C_{61} butyric acid methyl ester (PCBM) as the acceptor. Clear insight was gained by observing the efficient electron transfer from a polymer to fullerene, which was previously shown to take place on the femtosecond scale.[11] Although the dissociation of the primary photo-excitation, singlet excitons, was very efficient, the generated photocurrent was still rather low. Shaheen et al.[12] enhanced the efficiency of a PPV:PCBM BHJ system to 2.5% by selecting solvents with a higher boiling point, showing the great potential for this type of photovoltaic device. Padinger et al.[13] presented a further increase in the power conversion efficiency by using a blend of a poly(3-hexyl thiophene) donor (P3HT) in conjunction with PCBM. It was shown that thermal annealing at a temperature above the glass transition of the polymer enabled an enhancement of the efficiency from 0.4 to 3.5%. Recently, results have shown that the efficiency of the BHJ solar cell could be further increased by adding additives, which allow an increased control of the phase segregation during film formation of a polymer–fullerene blend, yielding an efficiency up to 6%.[14] In addition, the photoconversion efficiency of polymer solar cells PSC has increased from ∼2.5% in 2001 to >8% since 2011 or 10%, which was recently obtained through the development of new electron donor polymers.[15]

In this article, we will discuss the concepts to improve the efficiency of the BHJ solar cells and the effects of nanomorphology on the performance of solar cells. First, the device geometry of BHJ solar cells and several prospective low-bandgap polymers are reviewed. Second, the effects of processing parameters (film deposition, postheat treatment, effect of additives, and UV ozone treatment) on device performance are discussed. Finally, transient photoconductivity measurements are analyzed to study the charge transport in BHJ solar cells. A thorough understanding of the fundamentals of device optimization is required in order to expand their limits in the future.

2 Electronic Donor–Acceptor Interactions in Conjugated Polymer Composites for Solar Cell Applications

Figure 1 depicts a general schematic of polymer solar cells where the formation of excitons takes place upon exposure to light. Exciton diffusion length (L_D) and donor–acceptor interface are two major factors that determine the exciton diffusion efficiency (η_{ED}). Exciton diffusion length in conjugated polymers is in the range of 4 to 20 nm. These excitons will be dissociated into
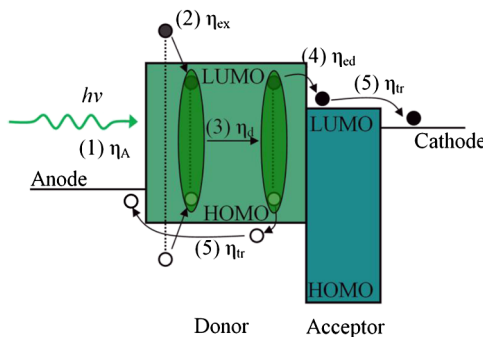

Fig. 1 Energy band diagram of polymer solar cells showing all processes of operation. Process: (1) photon absorption; (2) and (3) excitongeneration and diffusion; (4) exciton separation; (5) and (6) charge transport and collection. Reproduced with permission from Royal Society of Chemistry.[16]
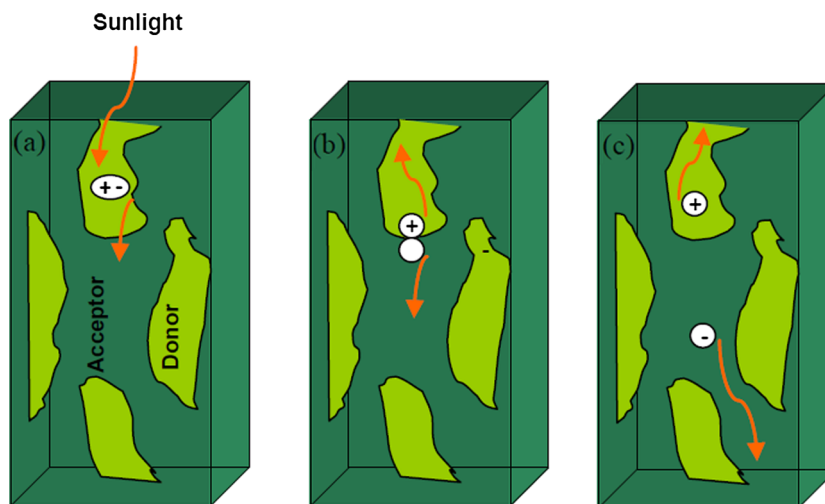
Fig. 2 Cartoon depicting separation of excitons into e-h pairs in polymer solar cell: (a) generation and diffusion of exciton, (b) dissociation of exciton, and (c) transport of e-h pairs. Reproduced with permission from South Dakota State University.[19]

electrons and holes when they reach the interface between the donor and acceptor. Thereafter, the separated charge carriers (electrons and holes) move toward their respective electrodes.

Conjugated polymers based on organic solar cell can be fabricated from low-cost solution processing techniques, including spin-coating, spray-coating, and ink-jet printing.[17,18] The mechanism for converting light into electricity in organic solar cells is governed by the absorption of photons in the active layer, which is followed by exciton formation, exciton diffusion, exciton dissociation, charge transport, and charge collection. Figure 2 shows the mechanism of photogenerated exciton formation upon light absorption, exciton dissociation at the donor–acceptor interface, and then transportation of the dissociated charges out of the film. Broad-bandgap polymers (1.3 to 1.4 eV) are selected for broad band light absoption to give high current density in solar cells.[4,16] The energy band offsets between donor and acceptor LUMOs should be in the range of 0.4 eV for efficient charge transfer between the donor and acceptor.[4,16] Optimized nanomorphology is required for both exciton diffusion and charge transport. The donor and acceptor phase separation should be in the range of ∼10 to 20 nm with a continuous pathway so that free carriers can efficiently transport to their corresponding electrodes.[4] Examples of donor/acceptor composites include P3HT or poly(diketo-pyrrolopyrrole-terthiophene) (PDPP3T)–fullerene derivatives {[6,6]-phenyl-C_{61}-butyric acid methyl ester ($PC_{60}BM$), [6,6]-phenyl-C_{71}-butyric acid methyl ester ($PC_{70}BM$), Indene-C60 bisadduct} and other combinations using low-bandgap polymers.

2.1 *Polymer–Fullerene Bulk Heterojunction Blends*

Most common polymers used in BHJ solar cells, including MEH-PPV,[20–23] poly[2-methoxy-5-(3′,7′-dimethyl-octyloxy)-1,4-phenylene vinylene],[24–28] P3HT,[29–33] PDPP3T,[34,35] and poly (cyclopentadithiophene-*alt*-benzothiadiazole),[36] are reported to form phase separated donor–acceptor blends with fullerene derivatives, such as $PC_{60}BM$ and $PC_{70}BM$. The optimization of the polymer–fullerene blend is based on tuning the electronic properties and interactions of the donor and acceptor components, which will generate large numbers of free charge carriers without significant loss. Proper understanding of electronic characteristics of the individual components (e.g., absorption coefficient, charge carrier mobility) helps to design next-generation high-efficiency solar cells.

Figure 3(a) shows a charge transfer from P3HT to PCBM. Figure 3(b) shows charge transfer from P3HT to $PC_{60}BM$ with LUMO (−3.2 eV), which is higher than that of PCBM (−4.2 eV) and has a sufficient energy offset for exciton dissociation and charge transfer between P3HT and PCBM. The bandgap of donor polymers need to be reduced to broaden the absorption. The commonly used polymer P3HT has absorption until 650 nm, which uses only 30% of the
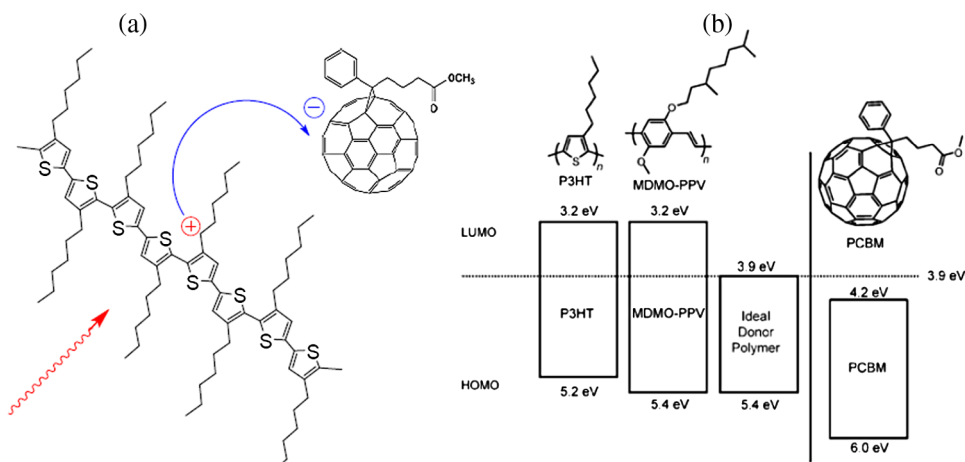
Fig. 3 (a) shows a charge transfer from P3HT to PCBM. (b) shows charge transfer from P3HT to PC$_{60}$BM with LUMO (−3.2 eV), which is higher than that of PCBM (−4.2 eV) and has a sufficient energy offset for exciton dissociation and charge transfer between P3HT and PCBM.

solar energy reaching the Earth. In addition, the HOMO/LUMO energy levels of P3HT are higher in comparison to fullerene derivatives. It is necessary to develop low-bandgap polymers with optimized energy band offsets. The low-bandgap polymers have the potential to absorb more sunlight, which leads to higher short-circuit current density (J_{sc}). The proper alignment of the HOMO/LUMO level of polymer and fullerene provides higher open-circuit voltage. Reports show that polymers with bandgaps of 1.2 to 1.5 eV have been developed.[5] Several novel polymers with HOMO/LUMO energy levels −5.5 and −3.6 eV, which is lower than the HOMO/LUMO energy levels of P3HT, have been synthesized.[37,38] Figure 4 is a nonexhaustive list of the molecular structures of various low-bandgap polymers, including chemical structure, HOMO, LUMO, bandgap, and their experimentally achieved efficiencies in single and multijunction devices. These lists of low-bandgap polymers will help researchers working in the field of organic PVs and perovskite solar cell to select an appropriate interconnecting layer.[5]

3 Effect of Processing Parameters and Morphology on Solar Cell Performance

The device architecture of a polymer solar cell consists of an electron and hole transport layer with the photoactive layer sandwiched between them. The photoactive layer may be a bilayer structure or BHJ structure.[51,52] In bilayer devices, different types of charge carriers (e.g., electrons or holes) travel independently within separate materials and bimolecular recombination is largely suppressed. However, the disadvantage is poor exciton dissociation and charge transfer due to the minimal donor–acceptor interface. This limitation was finally overcome by the concept of BHJ, where the donor and acceptor materials are intimately blended through the bulk. This helps in charge separation throughout the volume and within the exciton diffusion length. In order to build higher-efficiency devices, several processing parameters are taken into consideration. The processing parameters may include selection of solvents, blend ratio between polymer and fullerene, solution concentration, annealing temperature, spin speed (thickness), active layer treatment (solvent or thermal annealing), treatment to electron and hole transport layer (UV ozone treatment), deposition of electrode, and use of additives. Binary or ternary solvents in different volume ratios have also been studied to vary nanoscale morphology that has an effect on device performance.[53]

Different types of solvents have been used for processing the active layer in a BHJ solar cell. The morphology of the active layer varies with different types of solvents used, which affects the overall efficiency of solar cells. Some polymers are more soluble in one solvent whereas they are less soluble in others. Some polymers, like P3HT, increase their crystallinity after thermal annealing and show higher device performance. Upon thermal annealing, the chain of the polymer becomes mobile and the polymer becomes more organized to form an ordered structure. A
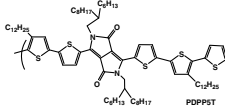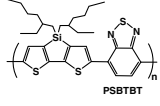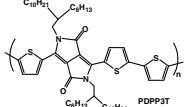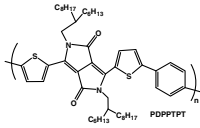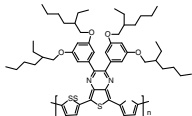
Structure	Name	HOMO (eV)	LUMO (eV)	Bandgap (eV)	Cell efficiency (%)		
					Single-junction	Multi-junction	Ref.
PDPP5T: poly(diketopyrrolopyrrole-quintetthiophene)		-5.12	-3.55	1.32	5.3	7.0	(38),(39)
PSBTBT: dithieno[3,2-*b*:2′,3′-*d*]silole polymer,poly[(4,4′-bis(2-ethylhexyl)dithieno[3,2-*b*:2′,3′-*d*]silole)-2,6-diyl-alt-(2,1,3-benzothiadiazole)-4,7-diyl]		-5.05	-3.27	1.45	4.7	7.0	(40),(41)
PDPP3T: poly(diketopyrrolopyrrole-terthiophene)		-5.17	-3.61	1.30	4.7	---	(42)
PDPPTPT: (poly[{2,5-bis(2-hexyldecyl)-2,3,5,6-tetrahydro-3,6-dioxopyrrolo[3,4-c]pyrrole-1,4-diyl}- *alt* - {[2,2′-(1,4-phenylene)bisthiophene]-5,5′-diyl}]		-5.35	-3.53	1.53	5.5	---	(43)
PTBEHT: poly(5,7-di-2-thienyl-2,3-bis(3,5-di(2-		----	----	1.2	1.1	0.57	(44)

Fig. 4 Nonexhaustive list of typical low-bandgap polymer donor materials in organic solar cells. Reproduced with permission from Royal Society of Chemistry.[5]

slow growth process called solvent annealing also affects the performance of P3HT. Li et al. showed that the ordered structure is destroyed due to the fast growth process.[54] Thus, the degree of self-ordering can be varied by controlling the film growth rate, i.e., the time it takes for the wet film to dry.

The study of Ngo et al.[55] based on spin-coating versus spray-coating is shown in Fig. 5(a). It provides a comparative study on the active layer deposition technique that plays a significant role in the film morphology. The phase image in Fig. 5(b) shows a self-assembled dotted polymer morphology in the active layer for spin-cast films and a fibrillar structure for spray-coated film. Self-assembled fibrillar structures were mainly found due to the longer evaporation time taken by the solvent. These fibrillar structures contribute to enhancing charge carrier mobility by providing fewer resistant charge transport pathways leading to a higher J_{sc} and fill factor.
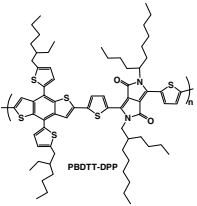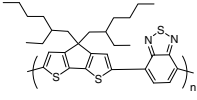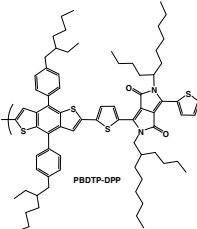
	ethylhexyloxy) phenyl)-thieno[3,4-b]pyrazine						
	PBDTT-DPP: poly{2,6'-4,8-di(5-ethylhexylthienyl)benzo[1,2-b;3,4-b]dithiophene-alt-5-dibutyloctyl-3,6-bis(5-bromothiophen-2-yl)pyrrolo[3,4-c]pyrrole-1,4-dione}	-5.30	-3.63	1.44	6.5	8.62	(45)
	PCPDTBT:poly[2,6-(4,4-bis-(2-ethylhexyl)-4*H*-cyclopenta[2,1-b;3,4-b']dithiophene-*alt*-4,7-(2,1,3-benzothiadiazole)]	-4.9	-3.5	1.4	3.2%	6.5%	(46, 47)
	PBDTP-DPP: poly{2,6'-4,8-di(5-ethylhexylthienyl)benzo[1,2-b;3,4-b]dithiophene-alt-5-dibutyloctyl-3,6-bis(5-bromothiophen-2-yl)pyrrolo[3,4-c]pyrrole-1,4-dione}	-5.35	-3.56	1.46	6.2	8.5	(48)

Fig. 4 (*Continued.*)

Ngo et al. also mentioned controlling the morphology of widely used ZnO as an electron transport layer (ETL) into more compact and smoother films. In the same work, they also mentioned that the morphology of widely used ZnO as an ETL could be controlled into a more compact and smoother film using the spray-coating technique. However, deposition of both the ETL and active layer via a spray-coating technique led to lower efficiency due to the poor interface formed between these two layers.

A study conducted by Adhikary et al. showed optimum UV ozone treatment time on sol gel prepared ZnO as ETL leads to an improved device performance of an inverted BHJ polymer solar cell.[56] They compared three different conditions of UV ozone exposure time on ZnO: unexposed, optimally exposed (5 min), and overexposed (20 min). The unexposed ZnO film was thought to be contaminated by organic residues originating from the sol gel method acting
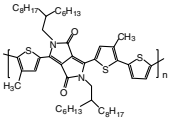
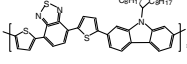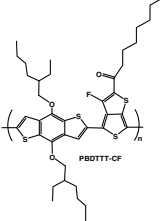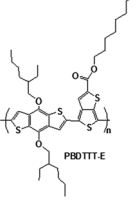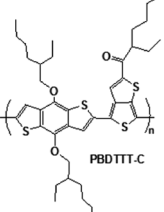| Structure	Name						
	PMDPP3T: poly[[2,5-bis(2-hexyldecyl-2,3,5,6-tetrahydro-3,6-dioxopyrrolo[3,4′c]pyrt role-1,4-diyl]-alt-[3′,3″-dimethyl-2,2′:5′,2″-terthiophene]-5,5″-diyl]	-----	-----	1.30	7.0	8.9 (2J) 9.64 (3J)	(49)
	PCDTBT: poly[N-9''-hepta-decanyl-2,7-carbazole-alt-5,5-(4',7'-di-2-thienyl-2',1',3'-benzothiadiazole)]	-5.5	-3.6	1.88	6.33	7.0	(37),(38)
	PBDTTT-CF: poly[4,8-bis-substituted-benzo[1,2-b:4,5-b0]dithiophene-2,6-diyl-alt-4-substituted-thieno[3,4-b]thiophene-2,6-diyl]-derived polymer	-5.22	-3.45	1.6	7.73	----	(50)
	PBDTTT-E: poly[4,8-bis-substituted-benzo[1,2-b:4,5-b0]dithiophene-2,6-diyl-alt-4-substituted-thieno[3,4-b]thiophene-2,6-diyl]-derived polymer	-5.01	-3.24	1.6	5.15	----	(50)
	PBDTTT-C: poly[4,8-bis-substituted-benzo[1,2-b:4,5-b0]dithiophene-2,6-diyl-alt-4-substituted-thieno[3,4-b]thiophene-2,6-diyl]-derived polymer	-5.12	-3.35	1.6	6.58	----	(50)

Fig. 4 (*Continued.*)

as recombination centers. Optimally exposed ZnO film yielded the highest device efficiency, while ZnO film exposed for a longer UV ozone treatment time led to the formation of p-type defects (oxygen interstitials) in ZnO. These defects push the ZnO Fermi level further away from the vacuum level and decrease the Wurtzite crystallinity, lowering the electron extraction efficiency of the layer and resulting in poor device efficiency.[6] The *JV* characteristics for three different UV ozone treatment conditions are shown in Fig. 6.

Power conversion efficiency has been correlated to the morphological control in BHJ solar cells, which has become a major part of organic solar cell research.[57–59] Favorable morphology has been suggested with adjustment of different processing parameters like thermal annealing, solvent vapor annealing, high boiling solvents, inorganic nanocrystals, and additives.[60] However, processing with solvent additives in addition to the primary host solvent has been found effective in improving active layer morphology.[60–62] Morphology of the organic solar cell active layer can be controlled with various additives, such as 1,8di-iodooctane (DIO), chloronepthlene (CN), 2,3
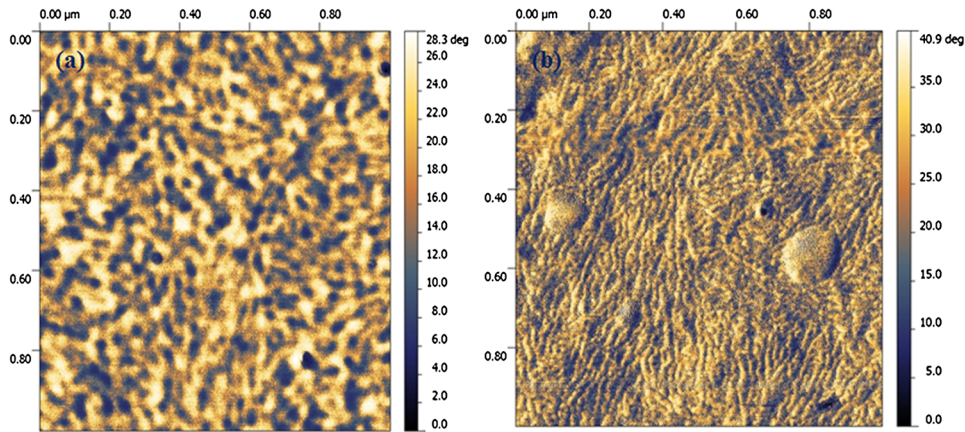
Fig. 5 Phase images indicating active layer deposited via (a) spin coating and (b) spray coating techniques. Reproduced with permission from Ref. 10.
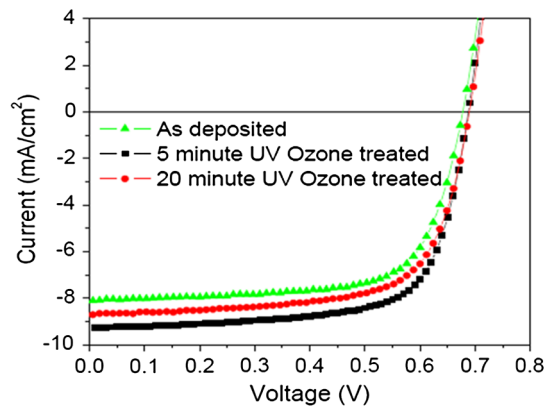

Fig. 6 $J - V$ curves for poly(diketo-pyrrolopyrrole-terthiophene) (PDPP3T): [6,6]-phenyl-C_{61}-butyric acid methyl ester (PC$_{60}$BM) inverted solar cell with different UV ozone treatment time on ZnO films. Reproduced with permission from Ref. 56.

pyridinediol, nitrobenzene, and octane dithiol (ODT). Solvent additives have been adopted and have been compatible with large-scale production. The additives induce better nanoscale phase separation[63–65] for the same or a similar polymer structure and also lead to higher domain purity or crystallinity in the polymer phase.[17] Investigation has been carried out on material selection, interpretation of the additive interaction with BHJ materials, and variation of morphology at different length scales. The role of solvent additives has been an important resource for further improving the efficiency of organic solar cells.

Two methods have been widely used in selecting host solvents and additives. (1) Host solvents usually possess a high solubility to both electron donor and acceptor molecules, whereas solvent additives have selectively higher solubility to one of the two components, typically with the acceptor. (2) Solvent additives are typically less volatile with a higher boiling point than the host solvent.[60,61] A different study has been conducted to remove the residual additives by slow drying, high vacuum treatment, or by washing with a low boiling point solvent additive, such as methanol, to enhance the performance of BHJ solar cells.[66] Crystal orientation, interlayer spacing, crystal size, and number of crystals depend upon the type of BHJ solar cells under study. It is observed that low vapor pressure solvent additives have a pronounced effect on enhancing crystallinity in most BHJs. In molecular systems, high crystallinity during processing obviously improves for carrier mobility and strong intermolecular interaction. Venkatesan et.al.[17] compared the effects of several additives on the morphology of the active layer. Results showed that CN and DIO additives gave an optimal morphology, which helped to increase the overall efficiency of BHJ solar cells. Charge transport and bimolecular recombination dynamics were correlated
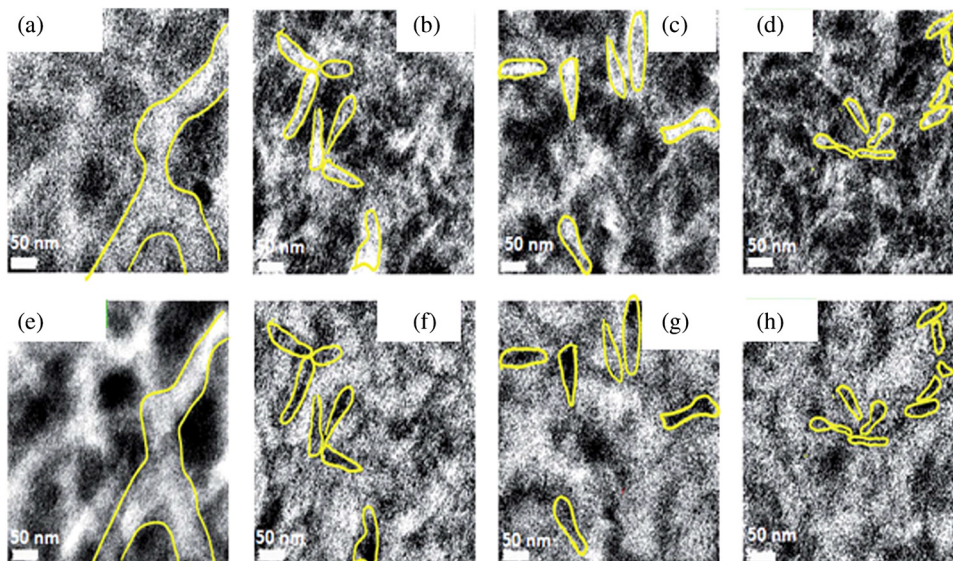
Fig. 7 (a) to (d) Energy field transmission electron microscopy (EFTEM) mapping of donor $(19 + 4 \text{ eV})$, and (e) to (h) EFTEM mapping of acceptor $(30 + 4 \text{ eV})$ for PDPP3T:PCBM films processed with [1,8di-iodooctane (DIO), chloronepthlene (CN), and octane dithiol (ODT)] and without additive (pristine), respectively. The bright regions (e.g., yellow marked) in the donor map [Fig. 6(a)] are also bright regions [Fig. 6(e)] in the acceptor map for pristine film. However, the film processed with DIO, CN, and ODT additive's bright regions [Figs. 6(b), 6(c), and 6(d)] correspond to the dark regions in the acceptor maps [Figs. 6(f), 6(g), and 6(h)].

with nanomorphology in polymer solar cells. Domain purity and domain size affect the charge transport and recombination dynamics.[67,68] Different characterizing tools have been used for insight study of nanoscale morphology. Atomic force microscopy, Kelvin probe force microscopy, transmission electron microscopy, energy field transmission electron microscopy (EFTEM), x-ray diffraction, soft x-ray scattering, grazing incidence wide-angle x-ray scattering, and selected area electron diffraction are basic characterizing tools for morphology study at the nanoscale range.

The effects of additives on nanoscale morphology revealed with EFTEM were shown in Fig. 7.[17] The EFTEM analysis gave deep insight into the local domain of both donor and acceptor phases. The donor and acceptor mapping for each type of film was compared. The donor polymer showed a bright region in $19 \pm 4 \text{ eV}$, whereas the acceptor fullerene showed bright spots in the corresponding $30 \pm 4 \text{ eV}$ due to the variation in their low-eV plasmon peak. Contrast inversion was not observed for a polymer–fullerene mixture without any additives showing a highly intermixed domain. On the contrary, contrast inversion was clearly observed for films processed with additives showing higher purity in either polymer-rich or acceptor-rich domains.

4 Charge Carrier Transport in Polymer Solar Cells

Charge transport and bimolecular recombination dynamics play an important role in the optimization of efficient polymer solar cells. In BHJ solar cells, ultrafast photoinduced charge transfer across the donor–acceptor interface takes place due to the absorption of incident light. These mobile electrons and holes are swept out and collected at the electrodes by the internal electric field, which is proportional to the magnitude of the internal field and limited by carrier mobility. Efficient charge transport across the respective electrodes takes place with the large donor and the acceptor interfacial area and percolating paths.[69]

The power conversion efficiency is limited by the recombination loss in the solar cells. Carrier collection by sweep-out to the electrodes and driven by the internal field must occur prior to carrier recombination within the cell.[70] Transient photocurrent (TPC) and photovoltage (TPV) measurements can provide insight into the physical mechanisms of solar cells. In

addition, it is necessary to understand and improve the charge carrier transport through the BHJ nanostructure for high-efficiency organic photovoltaic devices.

The main recombination process that limits solar cell performance is a nongeminate recombination loss.[71] The Langevin model is used to describe the second-order nongeminate recombination that takes place in these types of solar cells, which depends upon the concentration of free electrons and holes. The recombination rate is charge carrier mobility dependent and is related to these free carriers through the recombination coefficient. The variation of the apparent recombination order originates from device processing conditions, which leads to variations in the crystallinity of the photoactive layer causing different trap concentrations.[72] Therefore, the role of the polymer crystallinity on the bimolecular recombination order and defect density needs to be quantified.

TPV measurement is an optoelectronic technique in which devices are held at an open-circuit condition to measure the loss time of charge carriers with high input impedance of the oscilloscope.[73] The white light is used along with a laser pulse to create the open-circuit condition that depends on the background light intensity. After reaching some V_{oc} level, the short pulse of the dye laser is used to create a TPV under the open-circuit condition. The short laser pulse creates excess charge carrier density (Δn) with an increase in voltage (ΔV). The voltage decay in TPV acquired using 1 MΩ input impedance of oscilloscope is given by

$$\Delta V = V_{oc} + \Delta V_o \exp^{(-t/\tau)}, \tag{1}$$

where τ is the recombination time and V_{oc} is the open-circuit voltage.

TPC is a method where the device is held at the short-circuit condition with a short pulse applied to generate excess carrier across the device.[74] TPC gives the collection time of the carriers that are generated with a short pulse. The total charge carrier density can be calculated using TPC in conjugation with TPV. The transient current is obtained by calculating the current that flows through the small resistance using Ohm's law. The current decay in TPC acquired is given by

$$\Delta I = \Delta I_o \exp^{(-t/\tau)}, \tag{2}$$

where $\Delta I_o = \Delta V_o / R$, and R is the 20 Ω resistance used to put the device in a short-circuit condition.

The total charges that are generated can be calculated by integrating the current that is produced during the TPC technique:

$$\Delta Q = \int I \, dt. \tag{3}$$

The total charge carrier density is calculated using the differential capacitance, which is defined as

$$dc = \frac{\Delta Q}{\Delta V_o}, \tag{4}$$

where ΔQ is obtained from the TPC analysis, while ΔV_o is the amplitude of the TPV transient under different illumination conditions.

The total charge carrier density under certain illumination conditions is given by

$$n = \frac{1}{Aed} \int_0^{V_{oc}} c \, dV, \tag{5}$$

where e is the elementary charge, and A and d are the area and thickness of the device.

The recombination order ($\lambda + 1$) is inferred from the slope of the log-log plot of the small perturbation lifetime (t) versus the charge carrier density, which gives $-\lambda$ as

$$t \propto n^{-\lambda}, \tag{6}$$

where n is the charge carrier concentration.

The recombination coefficient K is given by

$$k(n) = -\frac{n^{\lambda-1}}{(\lambda+1)\tau_{\Delta n_o} n_o^{\lambda}}, \tag{7}$$

where $\tau_{\Delta n_o}$, n_o, and λ are determined experimentally.

Figures 8(a) and 8(b) show TPV and TPC decay for different donor/acceptor (D/A) ratios of poly2-octyldodecyloxy- benzo[1,2-b;3,4-b]dithiophene-alt-5,6-bis(dodecyloxy)-4,7-bis(dithiophen-2-yl)-benzo[c][1,2,5]-thiadiazole (PBDT-ABT-2/PCBM) BHJ solar cells. The TPV curves show that carrier recombination time or carrier lifetime (t_n) decreased with an increase in acceptor concentration in conjugated polymer/fullerene BHJ solar cells. This is similar to the previous results reported by Dennler et. al.[75] All the device shows a shorter charge transport time than the charge carrier lifetime.

The charge transport time is found to be ~422 ns for PBDT-ABT-2:PCBM BHJ solar cells with 1:1 D/A ratio. When the D/A ratio was changed from 1:1 to 1:2 and 1:0.5, the charge transport time was increased to 707 and 1316 ns. This is due to the fact that the charge transport time decreases with an increase in acceptor concentration as the percolation path along the acceptor increases. Moreover, the isolation of the polymer phase might have occurred by
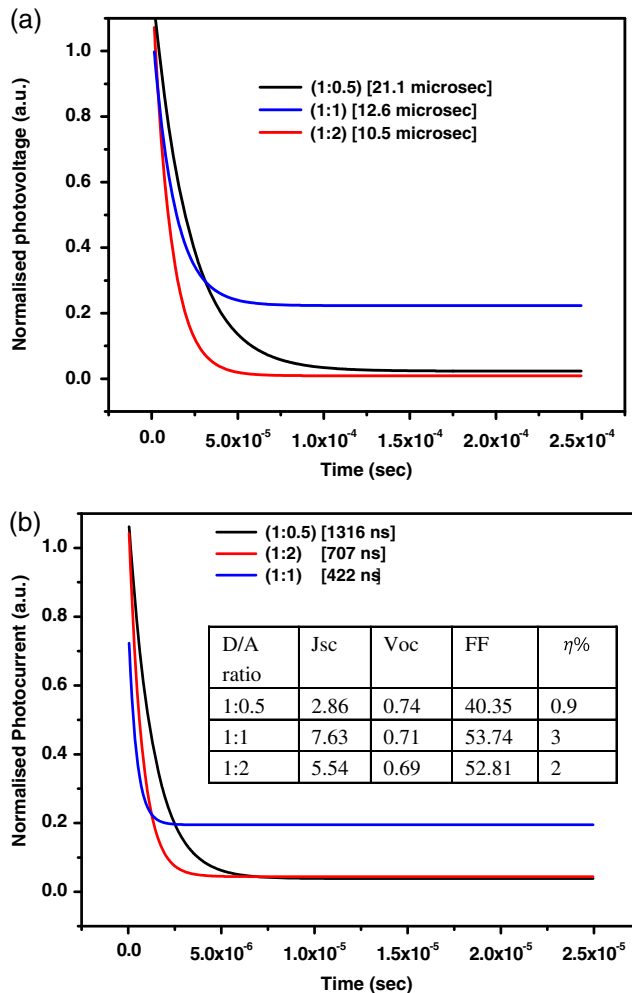

Fig. 8 (a) Normalized transient photovoltage and (b) normalized transient photocurrent for varying D/A ratio of PBDT-ABT-2/PCBM.
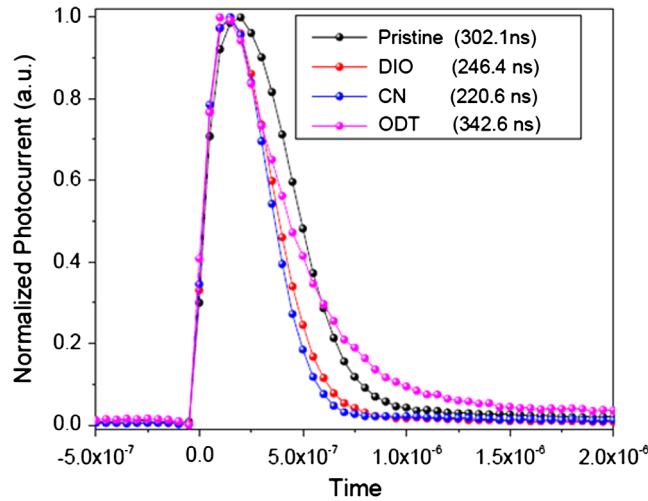
Fig. 9 Normalized transient photocurrent decay of PDPP3T: PC$_{60}$BM solar cells with different additives.

increasing the D/A ratio from 1:1 to 1:2, resulting in a longer charge transport time. The charge carrier lifetime calculated from the TPV decay curve is found to be longest for the 1:0.5 D/A rat Conjugated polymers io. In addition, the 1:0.5 D/A ratio also has the longest charge transport time compared to all other D/A ratios. From the above analysis, it can be concluded that the diffusion length (L_n), which is proportional to $\sqrt{\tau_n/\tau_d}$, depends upon the charge transport time and charge carrier lifetime.[9] Therefore, the 1:1 D/A ratio has the longest diffusion length and produces the highest performing device with a larger value for the short-circuit current density. Hence, transient measurements can be used to optimize the D/A ratio, which was found to be 1:1 for PBDT-ABT-2:PCBM BHJ solar cells.

A similar study has also been performed in PDPP3T:PCBM solar cells to investigate the effects of nanomorphology on charge transport with different additives and recombination behaviors in BHJ solar cells (Fig. 9).[17] It is found that the charge transport time for cells processed with CN and DIO additives is faster than those processed without additive and cells processed with ODT additive. The authors also preformed intensity-dependent transient analysis to understand the dependence of charge carrier lifetime on charge carrier concentration.
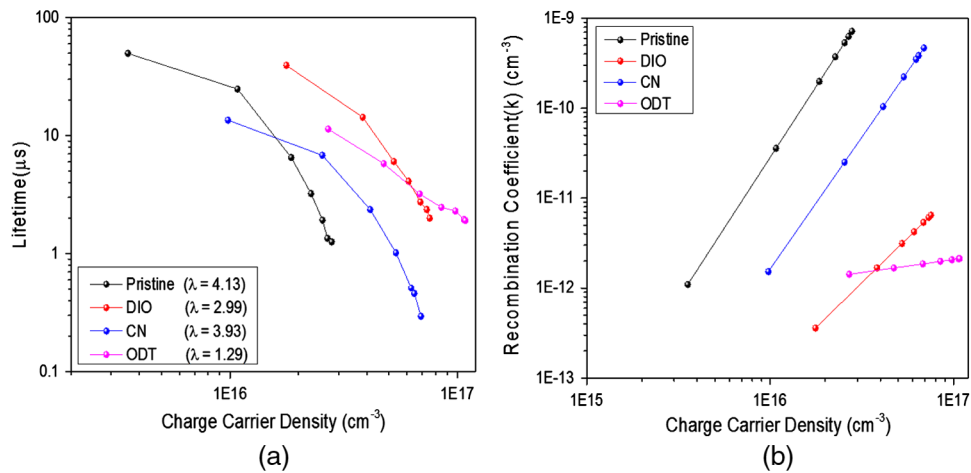

Fig. 10 (a) Apparent bimolecular recombination order (λ) obtained by fitting charge carrier lifetime versus charge carrier density of PDPP3T: PC$_{60}$BM solar cells with linear functions. (b) Dependence of bimolecular recombination coefficient on generated charge carrier density of PDPP3T: PC$_{60}$BM solar cells with varying intensity.

The dependence of charge carrier lifetime with charge carrier concentration of PDPP3T:PCBM solar cells with and without additives are shown in Fig. 10(a). The lifetime of the charge carrier follows the power law with charge carrier density given by $t \propto n^{-\lambda}$. This shows that the lifetime decreases with a higher charge carrier density. In addition, the slope (λ) obtained by fitting at higher intensities is greater for pristine, DIO, and CN processed cells, than cells processed with ODT additive. The slopes observed in Fig. 10 (a) ($\lambda > 1$) show that the recombination coefficient [Fig. 10 (b)] is charge carrier density dependent with the presence of traps in the bandgap and the trap density decreases with increasing crystallinity. In addition, the slope of ODT processed cells is smallest, resulting in the lowest bimolecular recombination.

5 Conclusion

Conjugated polymer–fullerene derivative based composites tend to provide a lot of advantages in terms of improvement in electronic property, stability, device engineering, and device performance without affecting the flexibility and ease of processability in fabricating organic solar cell devices. Morphological engineering can be done using solvent and solvent additives, which leads to different nanoscale morphologies in organic PVs. Processing parameters also play a major role in the evolution of different nanoscale morphologies, which has an effect on the overall device performance. The film formation process (spray-coating, spin-coating, and dip-coating) and post-treatment (UV ozone treatment and annealing) affect the physical properties, such as molecular configuration, miscibility, lateral and vertical phase separation, which changes the nanomorphology of the active layer. Transient photoconductivity measurement can be used to optimize the D/A ratio, which is found to be 1:1 for copolymer (PBDT-ABT-2):PCBM system. In addition, the recombination order and recombination coefficient provide insight on the understanding of the recombination that is dominant in prepared BHJ solar cells.

Acknowledgments

References

1. S. Glunz, R. Preu, and D. Biro, *Crystalline Silicon Solar Cells—State-of-the-Art and Future Developments*, Fraunhofer Institute for Solar Energy Systems, Freiburg, Germany (2012).
2. J. Selj et al., "Optimization of multilayer porous silicon antireflection coatings for silicon solar cells," *J. Appl. Phys.* **107**(7), 074904 (2010).
3. W. Zhang et al., "Oleamide as a self-assembled cathode buffer layer for polymer solar cells: the role of the terminal group on the function of the surfactant," *J. Mater. Chem.* **22**(45), 24067–24074 (2012).
4. M. K. Siddiki et al., "A review of polymer multijunction solar cells," *Energy Environ. Sci.* **3**(7), 867–883 (2010).
5. O. Adebanjo et al., "Triple junction polymer solar cells," *Energy Environ. Sci.* **6**(11), 3150–3170 (2013).
6. P. Adhikary et al., "Enhanced charge transport and photovoltaic performance of PBDTTT-CT/PC 70 BM solar cells via UV–ozone treatment," *Nanoscale* **5**(20), 10007–10013 (2013).
7. S. Sigdel et al., "Dye-sensitized solar cells based on spray-coated carbon nanofibers/TiO2 nanoparticles composite counter electrodes," *J. Mater. Chem. A* **2**, 11448–11453 (2014).
8. M. Shrestha et al., "Dual functionality of BODIPY chromophore in porphyrin-sensitized nanocrystalline solar cells," *J. Phys. Chem. C* **116**(19), 10451–10460 (2012).
9. P. P. Maharjan et al., "Photovoltaic devices and characterization of a dodecyloxybenzothiadiazole-based copolymer," *Phys. Chem. Chem. Phys.* **15**(18), 6856–6863 (2013).
10. G. Yu et al., "Polymer photovoltaic cells: enhanced efficiencies via a network of internal donor-acceptor heterojunctions," *Science* **270**(5243), 1789–1790 (1995).

11. C. Deibel, V. Dyakonov, and C. J. Brabec, "Organic bulk-heterojunction solar cells," *IEEE J. Sel. Topics Quantum Electron.* **16**(6), 1517–1527 (2010).
12. S. E. Shaheen et al., "2.5% efficient organic plastic solar cells," *Appl. Phys. Lett.* **78**(6), 841–843 (2001).
13. F. Padinger, R. S. Rittberger, and N. S. Sariciftci, "Effects of postproduction treatment on plastic solar cells," *Adv. Funct. Mater.* **13**(1), 85–88 (2003).
14. A. Hadipour, B. de Boer, and P. W. Blom, "Organic tandem and multi-junction solar cells," *Adv. Funct. Mater.* **18**(2), 169–181 (2008).
15. Z. He, H. Wu, and Y. Cao, "Recent advances in polymer solar cells: realization of high device performance by incorporating water/alcohol-soluble conjugated polymers as electrode buffer layer," *Adv. Mater.* **26**(7), 1006–1024 (2014).
16. X. Tingting and Q. Qiquan, "Conjugated polymer–inorganic semiconductor hybrid solar cells," *Energy Environ. Sci.* **4**, 2700–2720 (2011).
17. S. Venkatesan et al., "Interplay of nanoscale domain purity and size on charge transport and recombination dynamics in polymer solar cells," *Nanoscale* **6**(2), 1011–1019 (2013).
18. S. Venkatesan et al., "Polymer solar cells processed using anisole as a relatively nontoxic solvent," *Energy Technol.* **2**(3), 269–274 (2014).
19. T. Xu, *Novel Strategies to Prepare Polymer-Inorganic Hybrid Nanostructure Systems for Cost-Effective Energy Conversion*, Electrical Engineering and Computer Science Department, South Dakota State University, Diss, England (2012).
20. J. A. Ayllon and M. Lira-Cantu, "Application of MEH-PPV/SnO2 bilayer as hybrid solar cell," *Appl. Phys. A: Mater. Sci. Process.* **95**, 249–255 (2009).
21. A. J. Breeze, Z. Schlesinger, and S. A. Carter, "Charge transport in TiO2/MEH-PPV polymer photovoltaics," *Phys. Rev. B* **64**, 125205 (2001).
22. J. J. Dittmer et al., "Photovoltaic properties of MEH-PPV/PPEI blend devices," *Synth. Met.* **102**(1–3), 879–880 (1999).
23. N. C. Greenham, X. Peng, and A. P. Alivisatos, "A CdSe nanocrystal/MEH-PPV polymer composite photovoltaic," in *Proc. of Future Generation Photovoltaic Technologies: First NREL Conf.*, Vol. **404**, pp. 295–301, AIP Publishing (1997).
24. H. Hoppe et al., "Efficiency limiting morphological factors of MDMO-PPV:PCBM plastic solar cells," *Thin Solid Films* **511–512**, 587–592 (2006).
25. T. Martens et al., "Disclosure of the nanostructure of MDMO-PPV:PCBM bulk hetero-junction organic solar cells by a combination of SPM and TEM," *Synth. Met.* **138**(1–2), 243–247 (2003).
26. M. T. Rispens et al., "Influence of the solvent on the crystal structure of PCBM and the efficiency of MDMO-PPV:PCBM 'plastic' solar cells," *Chem. Commun.* **17**, 2116–2118 (2003).
27. T. Munters et al., "A comparison between state-of-the-art 'gilch' and 'sulphinyl' synthesised MDMO-PPV/PCBM bulk hetero-junction solar cells," *Thin Solid Films* **403–404**, 247–251 (2002).
28. P. A. van Hal et al., "Photoinduced electron transfer and photovoltaic response of a MDMO-PPV: TiO2 bulk-heterojunction," *Adv. Mater.* **15**(2), 118–121 (2003).
29. M. Al-Ibrahim et al., "Comparison of normal and inverse poly(3-hexylthiophene)/fullerene solar cell architectures," *Sol. Energy Mater. Sol. Cells* **85**(2), 277–283 (2005).
30. R. de Bettignies et al., "Study of P3HT:PCBM bulk heterojunction solar cells: influence of components ratio and of the nature of electrodes on performances and lifetime," *Proc. SPIE* **5938**, 59380C (2005).
31. B. A. Collins, J. R. Tumbleston, and H. Ade, "Miscibility, crystallinity, and phase development in P3HT/PCBM solar cells: toward an enlightened understanding of device morphology and stability," *J. Phys. Chem. Lett.* **2**(24), 3135–3145 (2011).
32. J. U. Lee et al., "Synthesis of C60-end capped P3HT and its application for high performance of P3HT/PCBM bulk heterojunction solar cells," *J. Mater. Chem.* **20**(16), 3287–3294 (2010).
33. R. A. Marsh et al., "Effect of annealing on P3HT:PCBM charge transfer and nanoscale morphology probed by ultrafast spectroscopy," *Nano Lett.* **10**(3), 923–930 (2010).
34. L. Ye et al., "From binary to ternary solvent: morphology fine-tuning of D/A blends in PDPP3T-based polymer solar cells," *Adv. Mater.* **24**(47), 6335–6341 (2012).

35. P. Adhikary et al., "Enhanced performance of PDPP3T/PC60BM solar cells using high boiling solvent and UV - ozone treatment," *IEEE Trans. Electron Devices* **60**(5), 1763–1768 (2013).

36. Y. Zhou et al., "Efficiency enhancement for bulk-heterojunction hybrid solar cells based on acid treated CdSe quantum dots and low bandgap polymer PCPDTBT," *Sol. Energy Mater. Sol. Cells* **95**(4), 1232–1237 (2011).

37. Y. Sun et al., "Inverted polymer solar cells integrated with a low-temperature-annealed sol-gel-derived ZnO film as an electron transport layer," *Adv. Mater.* **23**, 1679–1683 (2011).

38. V. S. Gevaerts et al., "Solution processed polymer tandem solar cell using efficient small and wide bandgap polymer:fullerene blends," *Adv. Mater.* **24**(16), 2130–2134 (2012).

39. Z. Yi et al., "Diketopyrrolopyrrole-based π-conjugated copolymer containing β-unsubstituted quintetthiophene unit: a promising material exhibiting high hole-mobility for organic thin-film transistors," *Chem. Mater.* **24**(22), 4350–4356 (2012).

40. J. Hou et al., "Synthesis, characterization, and photovoltaic properties of a low band gap polymer based on silole-containing polythiophenes and 2,1,3-benzothiadiazole," *J. Am. Chem. Soc.* **130**(48), 16144–16145 (2008).

41. J. Yang et al., "A robust inter-connecting layer for achieving high performance tandem polymer solar cell," *Adv. Mater.* **23**, 3465–3470 (2011).

42. J. C. Bijleveld et al., "Poly(diketopyrrolopyrrole-terthiophene) for ambipolar logic and photovoltaics," *Am. Chem. Soc.* **131**, 16616–16617 (2009).

43. J. C. Bijleveld et al., "Efficient solar cells based on an easily accessible diketopyrrolopyrrole polymer," *Adv. Energy Mater.* **22**, E242–E246 (2010).

44. M. M. Wienk et al., "Low-band gap poly(di-2-thienylthienopyrazine):fullerene solar cells," *Appl. Phys. Lett.* **88**(15), 153511 (2006).

45. L. Dou et al., "Tandem polymer solar cells featuring a spectrally matched low-bandgap polymer," *Nat. Photonics* **6**, 180–185 (2012).

46. J. Y. Kim et al., "Efficient tandem polymer solar cells fabricated by all-solution processing," *Science* **317**(5835), 222–225 (2007).

47. D. Mühlbacher et al., "High photovoltaic performance of a low-bandgap polymer," *Adv. Mater.* **18**(21), 2884–2889 (2006).

48. L. Dou et al., "Systematic investigation of benzodithiophene- and diketopyrrolopyrrole-based low-bandgap polymers designed for single junction and tandem polymer solar cells," *J. Am. Chem. Soc.* **134**(24), 10071–10079 (2012).

49. P. Joshi et al., "Electrospun carbon nanofibers as low-cost counter electrode for dye-sensitized solar cells," *ACS Appl. Mater. Interfaces* **2**(12), 3572–3577 (2010).

50. H.-Y. Chen et al., "Polymer solar cells with enhanced open-circuit voltage and efficiency," *Nat. Photonics* **3**(11), 649–653 (2009).

51. P. W. Blom et al., "Device physics of polymer: fullerene bulk heterojunction solar cells," *Adv. Mater.* **19**(12), 1551–1566 (2007).

52. S. Günes, H. Neugebauer, and N. S. Sariciftci, "Conjugated polymer-based organic solar cells," *Chem. Rev.* **107**(4), 1324–1338 (2007).

53. L. Ye et al., "From binary to ternary solvent: morphology fine-tuning of D/A blends in PDPP3T-based polymer solar cells," *Adv. Mater.* **24**(47), 6335–6341 (2012).

54. G. Li et al., "High-efficiency solution processable polymer photovoltaic cells by self-organization of polymer blends," *Nat. Mater.* **4**(11), 864–868 (2005).

55. E. Ngo et al., "Polymer photovoltaic performance and degradation on spray and spin coated electron transport layer and active layer," *IEEE Trans. Electron Devices* **60**(7), 2372–2378 (2013).

56. P. Adhikary et al., "Enhanced performance of PDPP3T/solar cells using high boiling solvent and UV-ozone treatment," *IEEE Trans. Electron Devices* **60**(5), 1763–1768 (2013).

57. M. Campoy-Quiles et al., "Morphology evolution via self-organization and lateral and vertical diffusion in polymer: fullerene solar cell blends," *Nat. Mater.* **7**(2), 158–164 (2008).

58. R. Fitzner et al., "Correlation of π-conjugated oligomer structure with film morphology and organic solar cell performance," *J. Am. Chem. Soc.* **134**(27), 11064–11067 (2012).

59. J. Guo et al., "Structure, dynamics, and power conversion efficiency correlations in a new low bandgap polymer: PCBM solar cell," *J. Phys. Chem. B* **114**(2), 742–748 (2010).

60. H.-C. Liao et al., "Additives for morphology control in high-efficiency organic solar cells," *Mater. Today* **16**(9), 326–336 (2013).
61. J. K. Lee et al., "Processing additives for improved efficiency from bulk heterojunction solar cells," *J. Am. Chem. Soc.* **130**(11), 3619–3623 (2008).
62. S. J. Lou et al., "Effects of additives on the morphology of solution phase aggregates formed by active layer components of high-efficiency organic solar cells," *J. Am. Chem. Soc.* **133**(51), 20661–20663 (2011).
63. Y. Yao et al., "Effects of solvent mixtures on the nanoscale phase separation in polymer solar cells," *Adv. Funct. Mater.* **18**(12), 1783–1789 (2008).
64. H. Hoppe et al., "Nanoscale morphology of conjugated polymer/fullerene-based bulk-heterojunction solar cells," *Adv. Funct. Mater.* **14**(10), 1005–1011 (2004).
65. M. Kim et al., "Electrical performance of organic solar cells with additive-assisted vertical phase separation in the photoactive layer," *Adv. Energy Mater.* **4**(2) (2014).
66. L. Ye et al., "Remove the residual additives toward enhanced efficiency with higher reproducibility in polymer solar cells," *J. Phys. Chem. C* **117**(29), 14920–14928 (2013).
67. B. P. Lyons, N. Clarke, and C. Groves, "The relative importance of domain size, domain purity and domain interfaces to the performance of bulk-heterojunction organic photovoltaics," *Energy Environ. Sci.* **5**(6), 7657–7663 (2012).
68. S. V. Kesava et al., "Domain compositions and fullerene aggregation govern charge photogeneration in polymer/fullerene solar cells," *Adv. Energy Mater.* **4**(11), (2014).
69. W. L. Leong et al., "Manifestation of carrier relaxation through the manifold of localized states in PCDTBT: PC60BM bulk heterojunction material: the role of PC84BM traps on the carrier transport," *Adv. Mater.* **24**(17), 2273–2277 (2012).
70. S. R. Cowan et al., "Transient photoconductivity in polymer bulk heterojunction solar cells: competition between sweep-out and recombination," *Phys. Rev. B* **83**(3), 035205 (2011).
71. P. Langevin, "Recombinaison et mobilites des ions dans les gaz," *Ann. Chim. Phys.* **28**(433), 122 (1903).
72. D. Spoltore et al., "Effect of polymer crystallinity in P3HT: PCBM solar cells on band gap trap states and apparent recombination order," *Adv. Energy Mater.* **3**(4), 466–471 (2013).
73. C. Shuttle et al., "Experimental determination of the rate law for charge carrier decay in a polythiophene: fullerene solar cell," *Appl. Phys. Lett.* **92**(9), 3311 (2008).
74. B. O'Regan et al., "The effect of Al2O3 barrier layers in TiO2/dye/CuSCN photovoltaic cells explored by recombination and DOS characterization using transient photovoltage measurements," *J. Phys. Chem. B* **109**(10), 4616–4623 (2005).
75. G. Dennler et al., "Charge carrier mobility and lifetime versus composition of conjugated polymer/fullerene bulk-heterojunction solar cells," *Org. Electron.* **7**(4), 229–234 (2006).

Nirmal Adhikari received his bachelor's degree in electrical engineering from the Institute of Engineering, Tribhuv an University, Kathmandu, Nepal, in 2006 and completed his master's degree in materials and process of sustainable energetics from Tallinn University of Technology, Eastern Europe, in 2011. He is currently pursuing his doctoral degree in electrical engineering from South Dakota State University under the supervision of Dr. Qiquan Qiao. His major research is on the interface engineering of perovskite solar cells at nanoscale for efficient charge transport using Kelvin probe force microscopy (KPFM) and transient photoconductivity measurements.

Devendra Khatiwada received his master's degree in physics from Prithvi Narayan Campus, Tribhuvan University, Nepal, in 2009. He is currently pursuing his master's degree in electrical engineering from South Dakota State University under the supervision of Dr. Qiquan Qiao. His research work includes morphology study of polymer bulkheterojunction solar cells.

Ashish Dubey is a graduate student in electrical engineering at South Dakota State University, US. He received his master's degree in nanotechnology from Amity University, India. Currently he is carrying out his doctoral thesis work in Dr. Qiquan Qiao's group. His research work includes perovskite-based solar cells, organic-inorganic semiconductor hybrid solar cells, structural and morphological studies of donor-acceptor blend films, and their optical and electrical characterization.

Qiquan Qiao is an associate professor in the Department of Electrical Engineering and Computer Science at South Dakota State University (SDSU), where he established the Organic Electronics Laboratory. Current research focuses on polymer photovoltaics and dye-sensitized solar cell materials and devices. He received the 2014 F O Butler award for excellence in research, the 2012 College of Engineering Young Investigator award, the 2010 US NSF Career award, and the 2009 Bergmann Memorial award from the US-Israel Bi-National Science Foundation (BSF). During his graduate study, he received the 2006 American Society of Mechanical Engineers Solar Energy Division Graduate Student award and the 2006 Chinese Government award for outstanding students abroad.